ELSEVIER

Mathematical Biosciences 169 (2001) 1–14

Mathematical Biosciences

www.elsevier.com/locate/mbs

A simple 2D biofilm model yields a variety of morphological features

Slawomir W. Hermanowicz *

Department of Civil and Environmental Engineering, University of California, Berkeley, CA 94720-1710, USA

Received 10 April 2000; received in revised form 29 August 2000; accepted 10 October 2000

Abstract

A two-dimensional biofilm model was developed based on the concept of cellular automata. Three simple, generic processes were included in the model: cell growth, internal and external mass transport and cell detachment (erosion). The model generated a diverse range of biofilm morphologies (from dense layers to open, mushroom-like forms) similar to those observed in real biofilm systems. Bulk nutrient concentration and external mass transfer resistance had a large influence on the biofilm structure. © 2001 Elsevier Science Inc. All rights reserved.

Keywords: Biofilm model; Biofilm morphology; Cellular automata; External mass transfer; Erosion detachment

1. Introduction: biofilms and their models

Biofilms are a common form of microbial ecosystems associated with surfaces. They are found in extremely varied environments from 'pure' water systems to stream beds, ship hulls and teeth surface. In response to varying environmental conditions, biofilms develop different structures expressed in various morphologies. The richness of morphological forms has been recognized by many researchers (e.g., [1–7]). However, characterization of biofilm morphology has been primarily restricted to qualitative descriptors such as 'smooth', 'fuzzy', 'mushroomlike'. Recently, quantitative descriptors have been proposed including porosity and its gradients [8], connected porosity [9] and fractal dimensions [9–11]. These attempts are still in the developmental stage and it is likely that biofilm morphology can be quantified by more than one parameter. Better understanding of biofilm morphology is important not only for its characterization but for description of mass transfer inside and around biofilms. While experimental methods will ultimately

* Tel.: +1-510 642 0151; fax: +1-510 642 7483.
E-mail address: hermanowicz@ce.berkeley.edu (S.W. Hermanowicz).

0025-5564/01/$ - see front matter © 2001 Elsevier Science Inc. All rights reserved.
PII: S0025-5564(00)00049-3

reveal biofilm structure, mathematical models can be useful tools for investigation of the effects of different environmental conditions on biofilm development and its morphology.

Early mathematical models of biofilms were derived from similar models used in chemical engineering to describe diffusion and reaction in a porous catalyst particle (e.g., [12]). Biofilm was treated as a homogeneous matrix with uniformly distributed biochemical reactive sites. A nutrient penetrated through the matrix by molecular diffusion and was transformed into products according to a prescribed local, intrinsic reaction rate. Such models were developed initially for one-dimensional geometry implying a flat biofilm. Later, two-dimensional and three-dimensional models were introduced (for a recent mini-review, see Ref. [13]). Additional features were further incorporated such as multiple nutrients, multiple microbial species, variable biofilm density [14–20]. A majority of existing models assumed that the biofilm composition and thickness were constant and described only nutrient transport and transformations. Some newer models included biofilm development (growth, detachment) most commonly through a biomass displacement velocity that depended on the local microbial growth rate (see Ref. [17]). All these models, however, treated the biofilm as a continuum and were based on differential mass balances of various biofilm components. More important, biofilm morphology was prescribed in the models. In some models, biofilm morphology was explicitly stipulated (e.g., as a flat layer) while in other models specific assumptions were made about biofilm development (e.g., that the biomass displacement velocity is perpendicular to the substratum). In either case, the models were unable to describe complicated biofilm morphologies observed experimentally in many systems.

We propose that a new class of biofilm models is needed to overcome this deficiency. Recently such a new class based on the idea of cellular automata has been presented [21–23]. All these independently developed models subscribe to a similar philosophy but are different in details. In our work [22] we developed a simple model incorporating only an absolute minimum of assumptions necessary to describe realistically biofilm development. This minimalistic approach is founded on two premises. First, we postulate that only processes of biofilm development included in a model are those that are strictly necessary to yield realistic model outcomes, given the current state of knowledge. Second, modeler's preconceived notions about biofilm organization should be kept to a minimum. Such limitations are achieved better if the rules of biofilm development are local, i.e., they are formulated for a smallest set of model elements. If a model, which includes only a small set of features, adequately represents the reality of biofilm structure, we are more convinced that these features are universal and common to generic biofilms. While complex models might perform better in describing individual cases, they require additional parameters to achieve better fit. Then, they often lose predictive powers as the choice of appropriate coefficients becomes bewildering. Similar approach was advocated by Schweitzer [24]. He stated that for a model "it is important to find a level of description which on one hand considers the specific features of the system and reflects the origination of new qualities, but on the other hand is not flooded with microscopic details". From this point of view, cellular automata provide a suitable framework for model development.

2. Modeling aspects: cellular automata as a biofilm model

Cellular automata are a class of models in which an assembly of objects is allowed to change according to a set of rules. Each object, called a cell, can assume a state value from a prescribed

set. The state of the object is changed depending on its value and inputs of other connected objects according to prescribed rules, 'a transfer function'. Wolfram [25] presented a comprehensive description of cellular automata and their applications to many problems in science. In microbiology, the development of microbial colonies on agar colonies was previously described with cellular automata [26].

To serve our stated purpose, the model must be robust since the detailed description of microbial physiology in biofilms is not yet fully developed. However, certain common features of biofilm organization and development can be considered as universal, at least in a broad semi-quantitative sense. These features include:

- nutrient uptake and biomass growth;
- nutrient mass transfer inside and outside a biofilm;
- detachment of biofilm fragments.

The objective of this work is to show how these general features can lead to the development of diverse biofilm morphology. In particular, a set of simple development rules defined on a small scale (possibly as small as a single cell) results in the formation of self-organized structures.

2.1. Simple developmental rules

In the present work, the biofilm consists of discrete units ('grid cells') which are embedded in a two-dimensional grid. The grid is typically rectangular and constitutes a working space in which the modeled biofilm is allowed to develop. The states of each grid cell are zero or unity, corresponding to cells filled with water or biomass, respectively (Fig. 1). To avoid any confusion in the terminology, we will use the term 'grid cell' to represent a model unit and 'microbial cell' to refer to a real, living organism. The size of the grid cells x is an arbitrary parameter based primarily on the desired model spatial accuracy. Since all features of the simulated biofilm are related to the chosen cell size, the simulated structures can be simply scaled up or down through an appropriate value of x. Thus, the resulting simulated biofilms are scale-free and geometrically self-similar (in a

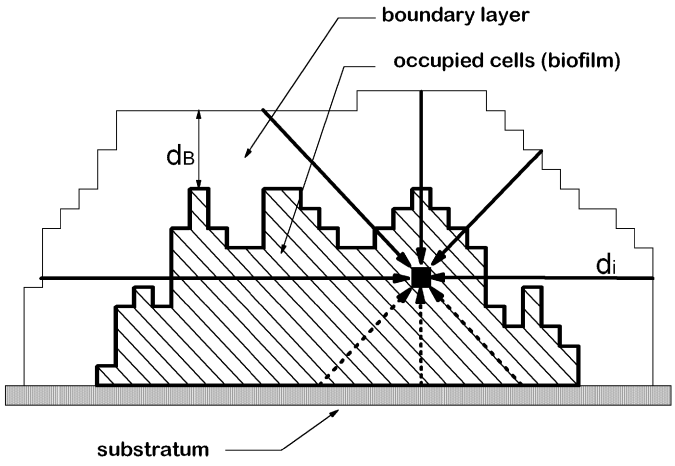

Fig. 1. Structure of the biofilm model (d_B – boundary layer thickness, d_i – penetration depth).

statistical sense). Hermanowicz and co-workers [9,10] found different morphological structures of a mixed-population, heterotrophic biofilm depending on their geometric scales. Small structures (less than approximately 5 μm) were very compact as characterized by their fractal dimension close to 2 (for 2-D cross-sections). Larger structures (with size above 10 μm) were much more open and possibly self-similar. Their 'fractal' dimension varied from 1.5 to 1.8 depending of the biofilm age, distance from the substratum and overall water flow direction. At present, it is not known whether these features are more commonly found in biofilms or what is the upper cutoff of the self-similarity. This type of analysis, however, could indicate an approximate size of smallest cell aggregates in a biofilm and suggest a suitable value of the cell model size x.

In our model, a matrix representing nutrient concentrations is superimposed on the working space containing water and biomass. In this work, only a single limiting nutrient was considered. Thus, the nutrient concentration matrix has the same dimensions as the working space grid. Biofilm development occurs in discrete time steps. At every time step, each occupied grid cell may divide with the probability P_d. In general, P_d can be a function of nutrient concentrations, cell metabolic status or other factors. In the present model, a simple Monod-like function was used to relate the probability P_d and the local limiting nutrient concentration c:

$$P_d = \frac{c}{c+K}. \tag{1}$$

Thus, at low nutrient concentrations, the grid cells will divide less frequently than at high nutrient concentrations. After each time step, the nutrient matrix is updated to describe a new nutrient concentration field. The updated concentration field reflects changes of nutrient uptake caused by new biofilm geometry. Nutrient concentration gradients result from a combination of nutrient uptake by the biomass and nutrient transport from the bulk fluid through a concentration boundary layer and inside the biofilm. The thickness of the concentration boundary layer adjacent to the biomass/water interface characterizes the external mass transport. In general, it depends on the flow regime. Zhang and Bishop [8] and DeBeer and co-workers [27] used microelectrodes to determine the nutrient concentration gradients and consequently the boundary layer thickness. DeBeer and co-workers [27] clearly demonstrated that the boundary layer thickness depended on the bulk water velocity. Yang and Lewandowski [28] also showed that mass transport outside the biomass clusters is much larger than inside the clusters. Presumably outside the clusters, advection dominates the transport while diffusion is the controlling factor inside the clusters.

In the model, a relatively simple representation of these processes was adopted. At each time step, (and thus at each step in biofilm development) a concentration boundary layer is imposed at the biofilm surface, i.e., for each occupied grid cell with at least one empty neighbor. The thickness of the boundary layer d_B is a model parameter and is expressed in the dimensionless form as $\delta_B = d_B/x$. It is assumed that mass transport through the boundary layer and inside the biomass (i.e., occupied grid cells) occurs by diffusion with the effective diffusion coefficient D (same for biomass and water). Outside the boundary layer, a constant nutrient concentration c_S is maintained (representing advection). In such a setup, a steady state concentration field can be described by a two-dimensional Poisson equation

$$D\nabla^2 c = r(c), \tag{2}$$

where $r(c)$ represents the intrinsic nutrient uptake rate. The appropriate boundary conditions are

$$c = c_S \quad \text{at the bulk/boundary layer interface,} \tag{3}$$

$$\left(\frac{dc}{dn}\right)_{n\perp S} = 0 \quad \text{at the substratum,} \tag{4}$$

where n is the direction perpendicular to the substratum S. Solving Eq. (2) with complicated geometry requires a lot of computational resources. In addition, Eqs. (2)–(4) still represent an idealization of a real biofilm. In the light of the previously expressed modeling philosophy, it seems that a simpler approach to calculate nutrient concentration distribution could be used as long as it describes a reasonably similar pattern of concentration gradients. This approach is quite different from the work of Picioreanu and co-workers [23] who solved numerically the full Poisson equation. For a flat, one-dimensional biofilm (and zero-order nutrient uptake kinetics) a concentration profile through a biofilm can be calculated by solving the one-dimensional version of Eq. (2) in an explicit form

$$c = \left[c_S^{1/2} - \left(\frac{kd^2}{2D}\right)^{1/2}\right]^2, \tag{5}$$

where k is the uptake rate and d is the distance from the surface of the biofilm (penetration distance). In an analogy with an electric circuit, one can consider that nutrient depletion is similar to a voltage drop across a resistor. The 'resistance' to mass transport is in this case a function of the penetration distance d. In a two-dimensional biofilm, nutrients can be supplied to a given point inside the biofilm in many directions from the biofilm surface. Again, in an analogy with resistor networks, the overall 'resistance' to mass transfer was approximated as a harmonic mean of 'resistances' in different directions. In the two-dimensional model, eight directions of nutrient supply were considered for each point inside the biofilm and the nutrient concentration was calculated from a 2-D analog of Eq. (5)

$$c = \left[c_S^{1/2} - \left(\frac{k}{2D}\left[\frac{1}{8}\sum_{i=1}^{8}\frac{1}{d_i^2}\right]^{-1}\right)^{1/2}\right]^2, \tag{6}$$

where d_i are penetration distances (see Fig. 1). Thus, at each time step, eight penetration depths d_i were calculated for each occupied grid cell and the corresponding nutrient concentration c was found from Eq. (6). Then, the probability of division for each occupied grid cell was computed from Eq. (1). The validity of this approach is assessed in Section 3.

The dividing cells must be accommodated in the model working space. In our work, we adopted a simple rule that governed the location of 'daughter' grid cells resulting from each grid cell division. If a dividing cell has one or more neighboring grid cells empty, the daughter cell occupies at random one of these empty cells. If no empty cells are available, the daughter grid cell must displace one of the occupied neighboring cells. The neighboring cell which offers the smallest mechanical resistance, i.e., laying in the direction of the shortest distance from the dividing cell to the biomass/liquid interface, is selected for the displacement (see Fig. 1). The displaced cell either occupies a neighboring empty space or pushes one of its occupied neighbors according to the same

rule if no empty space is available. Obviously, this rule is very simplistic and does not completely describe the behavior of a real biofilm. However, mechanisms governing displacement of dividing microbial cells in a real biofilm are not known. They probably include a combination of increasing local microbial cell density and displacement of biofilm components. Nonetheless, the proposed model rule might be a reasonable first step approximation. If mechanisms of microbial cell displacement in a real biofilm become known better, the rule may be modified and its effects on biofilm simulation reevaluated. In this capacity, a plausible biofilm model might be useful not only for formulating a specific hypothesis but also for its testing.

In addition to biomass growth and displacement, parts of the biofilm can detach from the rest of the matrix. Although this process appears to be very important for biofilm development, little is known about the phenomena which control biofilm detachment. Chang et al. [29], Peyton and Characklis [30], and Gjaltema and co-workers [31] reported biofilm detachment kinetics determined through multivariate regression analysis of several operational parameters. These correlations are of limited value for model development since they describe only case-specific average rates and not local detachment events. Other cell-based models [21,23] did not include detachment. Lacking any detailed information on local biofilm detachment, a very simple rule was again adopted in the present model. For grid cells at the biomass/liquid interface (i.e., for grid cells with at least one empty neighbor) the probability of cell erosion should be an increasing function of the hydrodynamic shear stress τ. In addition, the 'strength' of biofilm (its cohesion) should be also involved. We proposed to characterize this poorly defined feature with a single parameter σ. Thus, with an increasing biofilm strength σ, the probability of erosion should decrease. To accommodate this qualitative but intuitive description, the probability of cell erosion P_e was described by the following simple function:

$$P_e = \frac{1}{1 + (\sigma/\tau)}. \tag{7}$$

The probability P_e is shown in Fig. 2 as a function of σ and τ. Because the biofilm strength σ appears only as a ratio to the shear stress τ, there is no need for its physical interpretation. Simply, when $\sigma/\tau = 1$, the surface grid cells detach with the probability 1/2.

If, as a result of cell erosion, a cluster of cells became completely detached from the rest of the biofilm or the substratum, the whole cluster is eliminated from the work space. Such an erosion mechanism allowed for detachment of not only individual cells but also of larger clusters if their connections with the rest of the biomass of the substratum were severed. This feature was especially important for dendritic, ramified biofilm morphologies (see Fig. 4) where large clusters were often attached to the substratum with a narrow 'neck'.

Since the developed model includes only the most fundamental biofilm features and is used to describe a 'generic' biofilm, it is convenient to make all relevant parameters dimensionless. In this way, common features of various biofilms exposed to different environmental conditions can be investigated. In the further analysis the following transformations were applied: dimensionless nutrient concentration $C = c/K$, dimensionless boundary layer thickness $\delta_B = d_B/x$, dimensionless biofilm strength σ/τ and a dimensionless parameter $F = kx^2/2DK$. This last parameter is analogous to the Thiele modulus and represents the ratio of the nutrient uptake rate to the diffusional supply rate. In the proposed model, the development of the biofilm occurs through discrete steps and the time is not explicitly incorporated. However, the duration of each time step

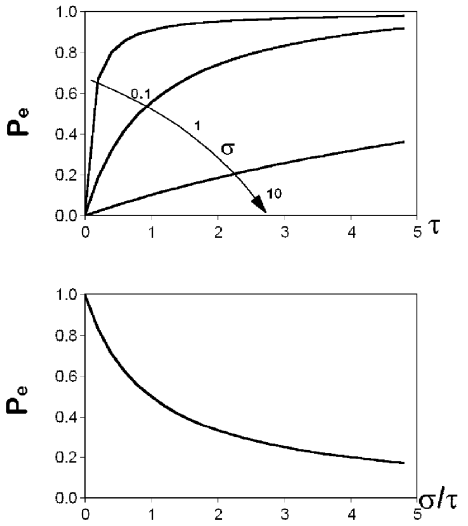

Fig. 2. Erosion probability P_e as a function of shear stress τ and biofilm 'strength' σ.

could be estimated from the following considerations. If for all occupied cells $c \gg K$, then the probability of division P_d is close to 1 (see Eq. (1)). Therefore, at each time step, all cells would divide and the biomass would double. It follows that the duration of a time step is comparable with the minimum doubling time $t_{min} = \ln 2/\mu_{max}$.

3. Computational methods

The developed model was implemented as a computer code using IDL language (RSI, Boulder, CO, USA) on a Windows 95 and NT platforms. The IDL language offers a few convenient features such as erosion and dilation functions which were used to create the boundary layer. For example, the boundary layer adjacent to a complex biomass/liquid interface (i.e., interface between occupied and empty grid cells) was created by dilating the set of occupied cells by the specified width. The dilation of the biomass was the result of a convolution of the working space matrix with a one dimensional row- or column-vector as a kernel. The length of the vector determined the thickness of the boundary layer. Erosion of the biomass is a dual function to the dilation of the void (unoccupied) space. The basis of the IDL procedures were described in [32]. Similarly, the interface itself could be determined by subtracting from the set of the occupied cells the same set eroded by one cell width. The connectivity function, also available in IDL, allowed for a convenient determination of cell clusters detached through the erosion of a single cell. Although IDL offered a convenient tool for model coding, any other suitable language can be used.

In the model, a simple analytical equation (Eq. (6)) was used to calculate the concentration in and around the biofilm. This approach was adopted because it simplified the program structure and dramatically decreased computational effort. The results were compared with the numerical solution of the full Poisson equation (Eq. (2)) which was solved on the same grid using a relaxation method. In this method, 10 000 steps were used to eliminate the influence of initial condi-

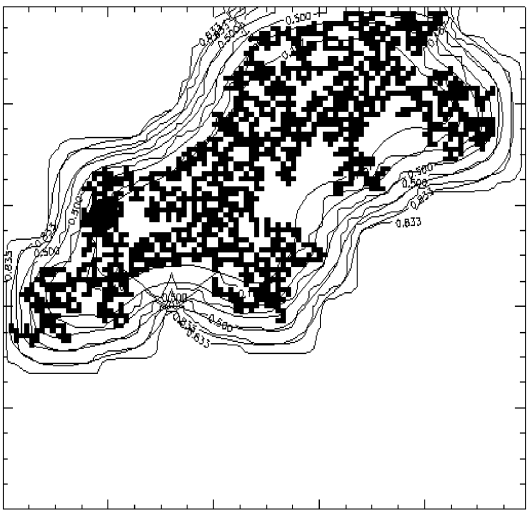

Fig. 3. Comparison of the numerical solution of the Poisson equation (smooth contours) with the simplified analytical solution (jagged contours) (see text for details).

tions. The results are shown in Fig. 3 for $F = 0.01$ and $C_S = 1$ for an irregular biofilm cluster. No flux boundary conditions were assumed at the substratum (top of the grid) and constant $C_S = 1$ for three remaining grid sides. Although the numerical solution was not identical with the simplified analytical equation, they coincided quite closely, certainly within any experimental accuracy.

Simulations were performed for grid sizes from 50×50 to 200×200 cells. Each simulation was terminated either after a specified number of steps (typically 50–100) or if the occupied cells filled more then 80% of the working space. The simulations were carried out for the following values of model parameters: $F = 0.01, 0.05, 0.1, 0.5$; $C_S = 1.5, 3, 5, 7, 9, 11, 13, 15$; $\delta_B = 1, 3, 5, 7, 9, 11$ and $\sigma/\tau = 0.1, 0.5, 1, 5$. Three repetitions were performed for each set of parameters yielding a total of 1152 simulations. For each of the simulated biofilms several morphological characteristics were determined including its porosity, surface extension and nutrient flux. Since the biofilm in each simulation grew to a different thickness, the porosity ε was defined as the fraction of unoccupied cells in a rectangle of the smallest height H_{min} wholly containing the biofilm

$$\varepsilon = 1 - \frac{N_{occupied}}{L_{substr}\, H_{min}}, \tag{8}$$

where $N_{occupied}$ is the number of the occupied grid cells in the work space, and L_{substr} is the length of the substratum in grid cell units. Internal porosity of the biofilm ε_I was defined as the fraction of unoccupied grid cells without connection to the bulk liquid. These cells were also counted in the smallest rectangle embedding the biofilm. Internal porosity ε_I is a measure of 'holes' in the biofilm which remain unfilled because of growth restrictions due to mass transfer limitations of the nutrient supply.

Picioreanu et al. [23] used surface enlargement SE as a measure to quantify biofilm morphology. In our work, we defined SE similarly as

$$\mathrm{SE} = \frac{L_{\mathrm{interface}}}{L_{\mathrm{substr}}}, \tag{9}$$

where $L_{\mathrm{interface}}$ is the length (in cell units) of the interface between occupied and empty grid cells. Typically, SE > 1 (sometimes SE $\gg 1$) due to irregular and convoluted biofilm interface. However, when the simulated biofilm was patchy and covered only a part of the substratum, SE could be less than 1.

4. Results and discussion

In our work, only four parameters, $C_S, \delta_B, \sigma/\tau$ and F were needed to describe biofilm development. Two of these, the dimensionless bulk nutrient concentration C_S and the dimensionless thickness of the boundary layer δ_B, can be controlled or easily monitored in a reactor thus exerting an external influence on biofilm development. Preliminary results reported earlier [33] suggested that the external mass transfer characterized by the boundary layer thickness greatly affected the morphology of the simulated biofilm. In this work, the effects of δ_B together with C_S, and σ/τ were further investigated. Fig. 4 displays one of the simulation results (for $F = 0.01$, $C_S = 2.6$, $\delta_B = 5$ and $\sigma/\tau = 0.2$). This figure shows the values of nutrient concentrations C, probability of division P_d and the cell age (i.e., the time step in which each cell was created by division). A concentration gradient is established through the boundary layer and the biofilm. As a result of these mass transfer limitations, cell divisions are predominantly in the outer zone of the biofilm. On the right side of the biofilm cluster a channel is open to advection since its width

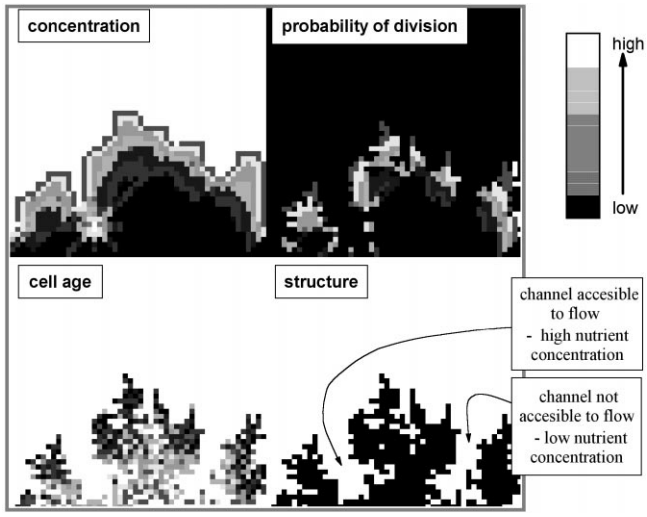

Fig. 4. An example of biofilm simulation ($F = 0.01, C_S = 2.6, \delta_B = 5, \sigma/\tau = 0.2$).

exceeds $2d_B$. On the left, only diffusional mass transport is possible because the channel width is smaller than $2d_B$.

Results of more simulations are shown in Fig. 5 which presents examples of biofilm morphology developed at different values of C_S, δ_B and σ/τ. These results are further quantified through surface enlargement SE, biofilm porosity ε, and inner porosity ε_I. Fig. 6 shows the evolution of surface enlargement SE in response to model parameters. Each of the six panels in Fig. 6 presents the changes of the evaluated variable (SE) in response to C_S for the specified value of δ_B. Similarly, Fig. 7 shows the variations of biofilm porosity ε, and Fig. 8 presents the inner porosity ε_I.

As seen in Fig. 5, the model was capable of producing a wide range of biofilm morphologies. These diverse structures were generated solely in response to changes of model parameters and not explicitly specified. Thus, the modeling results suggest that a few simple and generic processes in biofilm development can be responsible for greatly diversified biofilm structures observed in nature. An increase in the nutrient concentration C_S affects biofilm structure in a complex fashion. It is noteworthy that a small change of C_S can yield a very big difference in biofilm development. At low values of C_S, very little biofilm growth occurred. At best, only a few cells hugged the substratum while most growing cells were removed by erosion. For example, at $\delta_B = 1$ and $\sigma/\tau = 0.5$ (bottom left panel in Fig. 5) virtually no biofilm developed at $C_S = 1.5$. Initially deposited cells were unable to grow faster than they were removed from the substratum by erosion. Yet, a small increase of the nutrient concentration to $C_S = 3$, produced a dense layer of biomass. This major shift, reminiscent of a phase transition, is also seen in Fig. 6 where SE changes from almost 0 to approximately 2. Biofilm porosity also increased with the initial increase of C_S (Fig. 7). Biofilm strength (as represented by σ/τ) shifted the transition towards lower nutrient concentrations

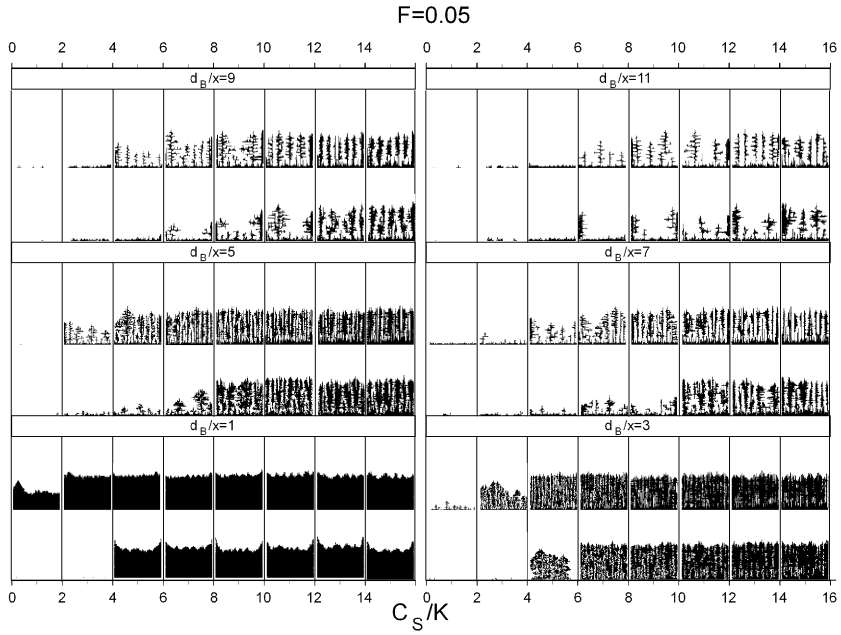

Fig. 5. Diverse biofilm morphologies generated by the model (top row in each panel: $\sigma/\tau = 5$, bottom row: $\sigma/\tau = 0.5$).

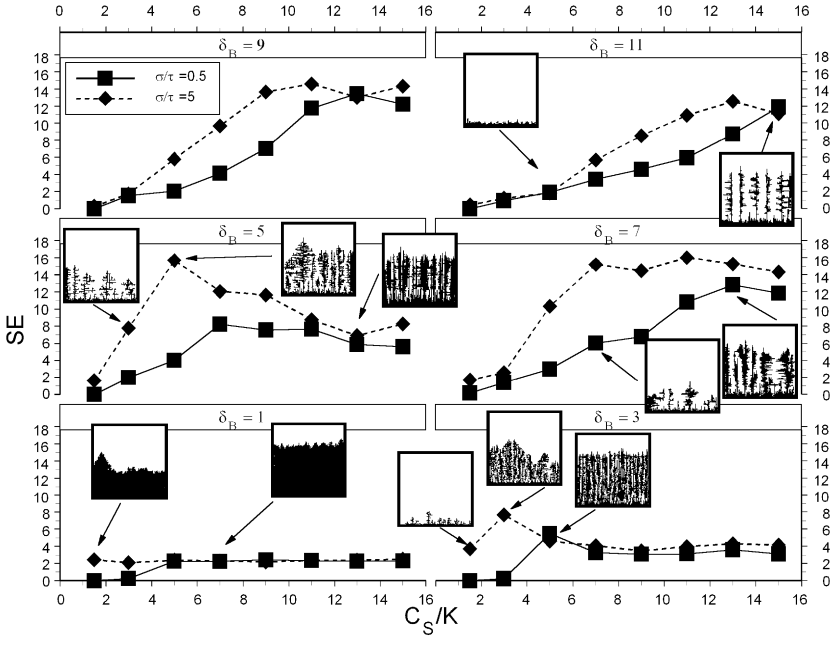

Fig. 6. Surface extension SE and examples of biofilm morphology for $F = 0.05$.

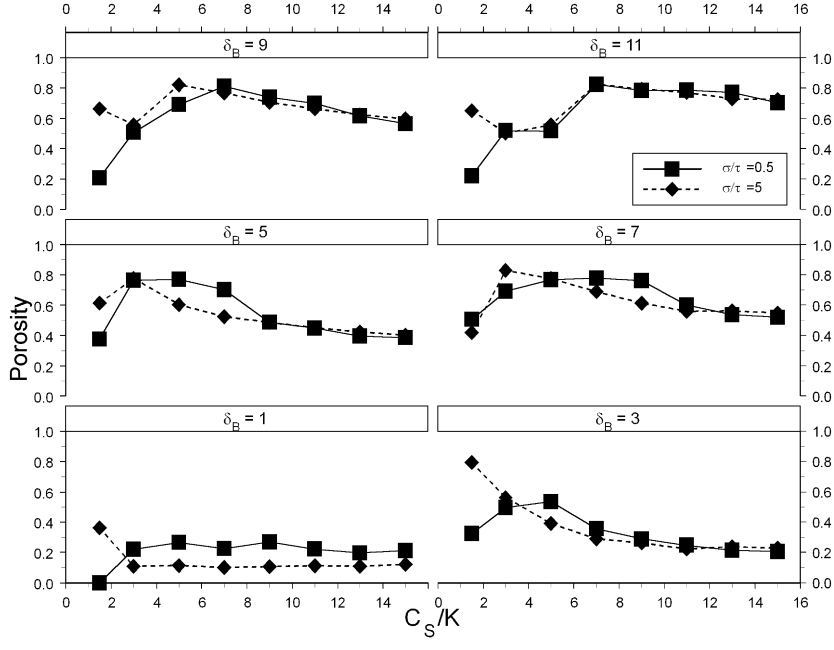

Fig. 7. Biofilm porosity for $F = 0.05$.

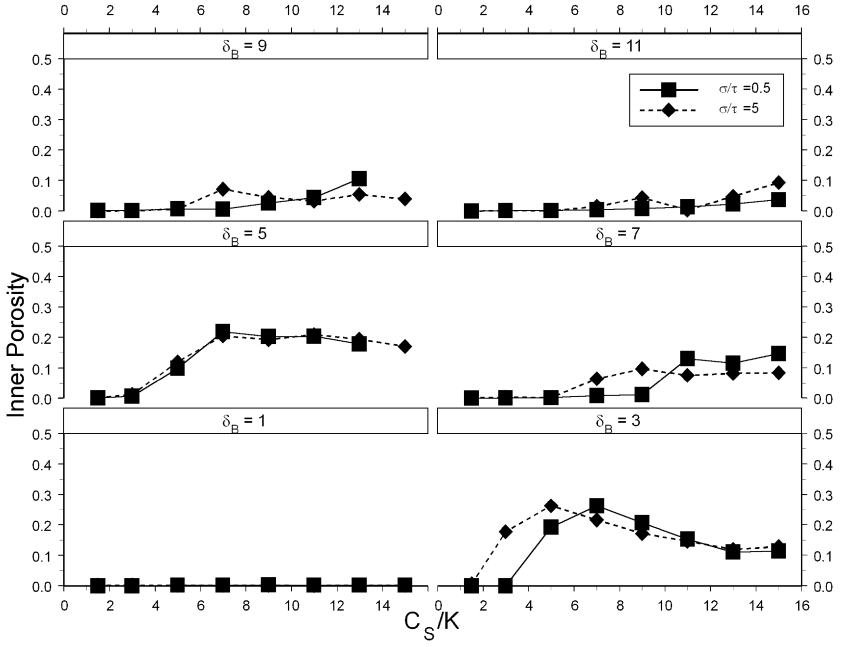

Fig. 8. Inner porosity of the biofilm for $F = 0.05$.

(compare the top and bottom rows in the bottom right panel in Fig. 5) but otherwise had little effect.

The transition from virtually no biofilm to an abundant biofilm was most pronounced at low δ_B (i.e., at low external mass transfer resistance). As δ_B was increased, the transition became more gradual with intermediate forms of biofilm appearing. Comparing biofilm morphology evolution at $\delta_B = 5$ (middle left panel in Fig. 5) with $\delta_B = 1$ (lower left panel in Fig. 5) illustrates this difference. Similarly, Fig. 6 shows a more gradual increase of SE at higher δ_B. As C_S continued to increase, both SE and ε reached a maximum and then decreased. At the highest nutrient concentrations, the biofilm became less porous and more compact due to increased nutrient penetration promoting growth inside the biofilm. Similarly, the highest inner porosity ε_I (Fig. 8) is realized at intermittent values of C_S when nutrient concentration is high enough for biofilm growth but, at the same time, not high enough to penetrate throughout the structure and supply nutrients to the inner holes. The concentration C_S at which biofilm porosity ε reached a maximum, shifted towards higher values for larger δ_B.

The changes of δ_B also have other effects on biofilm porosity ε (Fig. 7). At small δ_B (i.e., for small external mass transfer resistance), densely layered biofilms were developed. As δ_B increased, the biofilm developed in a more open, dendritic form. This phenomenon is typical to many diffusion-limited growth or aggregation processes (see [34]). Growth occurred primarily in the outer parts of the biofilms while the inner parts were shielded from nutrient supply and growth. These shielding effects of the boundary layer were less evident at higher nutrient concentrations C_S because more nutrient was available for growth even at higher mass transfer resistance.

Typically, the SE had a weak maximum in response to the variations of δ_B. At low δ_B, the interface length $L_{\text{interface}}$ of dense layered biofilms was only slightly bigger than $L_{\text{substratum}}$. With

increasing δ_B, the SE also increased as a result of the branching growth discussed previously. However, at very large δ_B the shielding effect resulted in the growth of individual 'trees' separated one from another. (Compare biofilm morphology $\delta_B = 5$ with that at $\delta_B = 11$.) Although each 'tree' was highly branched, the overall value of the interface area decreased due to their separation.

5. Conclusions

A biofilm model was developed using the cellular automata approach. The proposed model describes only the simplest case of a single-species biofilm with a single growth-limiting nutrient but the developed framework can easily be used for more complex modeling tasks. The results of modeling suggested that a small change of the bulk nutrient concentration can have a dramatic effect on the biofilm development. At the concentrations below the critical value, almost no biofilm can develop while at slightly higher concentrations, biofilm development is bountiful. This 'phase-like' transition is especially sharp for thin external boundary layers. Biofilm porosity and interfacial surface reach a maximum at an intermediate nutrient concentration. The value of this concentration tends to increase with thicker boundary layers.

The thickness of the boundary layer has a very strong influence on biofilm morphology. Thin boundary layers (hence low mass transfer resistance) promote the growth of dense and compact biofilms. At thicker boundary layers, much more open, dendritic biofilm forms develop, resembling 'mushrooms' or 'tulips' observed in some real systems. The effect of biofilm strength or cohesion have minor effects on its development.

The proposed model is capable not only of simulating a wide range of distinct biofilm morphologies but also suggesting that such diversity can possibly result from self-organization of small, individual units. The units evolve in accordance with a small set of minimally defined, local rules identical for all units. The differences in generated structures are not externally imposed but result from changes of very basic characteristics of the environment. Thus, the model can be a useful tool for the analysis of biofilm development.

References

[1] H. Siegrist, W. Gujer, Mass transfer mechanism in a heterotrophic biofilm, Water Res. 19 (1985) 1369.
[2] F.R. Christensen, G.H. Kristensen, J.L.C. Jansen, Biofilm structure – an important and neglected parameter in wastewater treatment, Water Sci. Technol. 21 (1989) 805.
[3] J.R. Lawrence, D.R. Korber, B.D. Hoyle, J.W. Costerton, D.E. Caldwell, Optical sectioning of microbial biofilms, J. Bacteriol. 173 (1991) 6558.
[4] S. Kugaprasatham, H. Nagaoka, S. Ohgaki, Effects of turbulence on nitrifying biofilms at nonlimiting substrate conditions, Water Res. 26 (1992) 1629.
[5] D. DeBeer, P. Stoodley, Z. Lewandowski, Liquid flow in heterogeneous biofilms, Biotechnol. Bioeng. 44 (1994) 636.
[6] A.A. Massoldeya, J. Whallon, R.F. Hickey, J.M. Tiedje, Channel structures in aerobic biofilms of fixedfilm reactors treating contaminated groundwater, Appl. Environ. Microbiol. 61 (1995) 769.
[7] P.S. Stewart, R. Murga, R. Srinivasan, D. DeBeer, Biofilm structural heterogeneity visualized by three microscopic methods, Water Res. 29 (1995) 2006.
[8] T.C. Zhang, P.L. Bishop, Density, porosity and pore structure of biofilms, Water Res. 28 (1994) 2267.

[9] S.W. Hermanowicz, U. Schindler, P. Wilderer, Fractal structure of biofilms: new tools for investigation of morphology, Water Sci. Technol. 32 (1995) 99.
[10] S.W. Hermanowicz, U. Schindler, P. Wilderer, Anisotropic morphology and fractal dimensions of biofilms, Water Res. 30 (1996) 753.
[11] W. Zahid, J. Ganczarczyk, Fractal properties of the RBC biofilm structure, Water Sci. Technol. 29 (1994) 217.
[12] P. Harremoes, Biofilms Kinetics. Water Pollution Microbiology, vol. 2, Wiley, New York, 1978, p. 71.
[13] D.R. Noguera, S. Okabe, C. Picioreanu, Biofilm modeling: present status and future directions, Water Sci. Technol. 39 (1999) 273.
[14] O. Wanner, W. Gujer, Multiple species biofilm model, Biotechnol. Bioeng. 28 (1986) 314.
[15] H. Furumai, B.E. Rittmann, Advanced modeling of mixed populations of heterotrophs and nitrifiers considering the formation and exchange of soluble microbial products, Water Sci. Technol. 26 (1992) 493.
[16] B.E. Rittmann, J.A. Manem, Development and experimental evaluation of a steady-state multispecies biofilm model, Biotechnol. Bioeng. 39 (1992) 914.
[17] O. Wanner, Modeling of mixed-population biofilm accumulation, in: G.G. Geesey, Z. Lewandowski, H.C. Flemming (Eds.), Biofouling and Biocorrosion in Industrial Water Systems, Lewis, Boca Raton, FL, 1994, p. 37.
[18] O. Wanner, New experimental findings and biofilm modelling concepts, Water Sci. Technol. 32 (1995) 133.
[19] O. Wanner, P. Reichert, Mathematical modeling of mixed-culture biofilms, Biotechnol. Bioeng. 49 (1996) 172.
[20] D.R. Noguera, G. Pizarro, D. Stahl, B.E. Rittmann, Simulation of multispecies biofilm development in three dimensions, Water Sci. Technol. 39 (1999) 123.
[21] J.W.T. Wimpenny, R. Colasanti, A unifying hypothesis for the structure of microbial biofilms based on cellular automaton models, FEMS Microbiol. Ecol. 22 (1997) 1.
[22] S.W. Hermanowicz, A model of two-dimensional biofilm morphology, in: Proceedings of the Second International Conference on Microorganisms in Activated Sludge and Biofilm Processes, University of California, Berkeley, CA, 21–23 July 1997; Water Sci. Technol. 37 (1997) 219.
[23] C. Picioreanu, M.C.M. Van Loosdrecht, J.J. Heijnen, Mathematical modeling of biofilm structure with a hybrid differential-discrete cellular automaton approach, Biotechnol. Bioeng. 58 (1998) 101.
[24] F. Schweitzer, Self-organization of complex structures from individual to collective dynamics – some introductory remarks, in: F. Schweitzer (Ed.), Self-organization of Complex Structures from Individual to Collective Dynamics, Gordon and Breach, London, 1997, p. xix.
[25] S. Wolfram, Theory and Applications of Cellular Automata, World Scientific, Singapore, 1986.
[26] E. Ben-Jacob, I. Cohen, Adaptive self-organization of bacterial colonies, in: F. Schweitzer (Ed.), Self-organization of Complex Structures from Individual to Collective Dynamics, Gordon and Breach, London, 1997, p. 243.
[27] D. DeBeer, P. Stoodley, P.Z. Lewandowski, Liquid flow and mass transport in heterogeneous biofilms, Water Res. 30 (1996) 2761.
[28] S. Yang, Z. Lewandowski, Measurement of local mass transfer coefficient in biofilms, Biotechnol. Bioeng. 48 (1995) 737.
[29] H.T. Chang, B.E. Rittmann, D. Amar, R. Heim, Biofilm detachment mechanisms in a liquid-fluidized bed, Biotechnol. Bioeng. 38 (1991) 499.
[30] B.M. Peyton, W.G. Characklis, A statistical analysis of the effect of substrate utilization and shear stress on kinetics of biofilm detachment, Biotechnol. Bioeng. 41 (1993) 728.
[31] A. Gjaltema, L. Tijhuis, M.C.M. van Loosdrecht, J.J. Heijnen, Detachment of biomass from suspended nongrowing spherical biofilms in airlift reactors, Biotechnol. Bioeng. 46 (1995) 258.
[32] R.M. Haralick, S.R. Sternberg, X.H. Zhuang, Image-analysis using mathematical morphology, IEEE Trans. Pattern Anal. Machine Intell. 9 (1987) 532.
[33] S.W. Hermanowicz, A model of two-dimensional biofilm morphology, Water Sci. Technol. 37 (1998) 219.
[34] T. Vicsek, Fractal Growth Phenomena, 2nd Ed., World Scientific, Singapore, 1992.